

# Distributed Zero-Forcing Amplify-and-Forward Beamforming for WSN Operation in Interfered and Highly-Scattered Environments

Slim Zaidi\*, Oussama Ben Smida<sup>†</sup>, Sofène Affes<sup>†</sup>, and Shahrokh Valaee\*

\*ECE Department, University of Toronto, Toronto, Ontario, M5S 3G4, Canada, Email: {slim.zaidi, valaee}@utoronto.ca

<sup>†</sup>INRS-EMT, Université du Québec, Montreal, QC, H5A 1K6, Canada, Email: {oussama.ben.smida,affes}@emt.inrs.ca

**Abstract**—In this paper, amplify-and-forward beamforming (AFB) is considered to establish a communication, through a wireless sensor networks (WSN) of  $K$  sensor nodes, from a source to a receiver in the presence of both scattering and interference. All sources send their data to the WSN during the first time slot while the nodes forward a properly weighted version of their received signals during the second slot. These weights are properly selected to maximize the desired power while completely canceling the interference signals. We show, however, that they depend on information locally unavailable at each node, making the zero-forcing beamformer (ZFB) unsuitable for WSNs, due to the prohibitive data exchange overhead and power depletion it would require. To address this issue, we exploit the asymptotic expression at large  $K$  of the ZFB weights that is locally computable at every node and, further, well-approximates their original counterparts. The performance of the resulting new distributed ZFB (DZFB) version is analyzed and compared to the conventional ZFB and two other distributed AFB benchmarks: the monochromatic (i.e., single-ray) AFB whose design neglects the presence of scattering and the bichromatic AFB which relies on an efficient two-ray channel approximation valid only for low angular spread (AS). We show that the proposed DZFB outperforms its monochromatic and bichromatic counterparts while incurring much less overhead and power depletion than ZFB. We show also that it is able to provide optimal performance even in highly-scattered environments as the latter.

**Index Terms**—Amplify-and-forward (AF) beamforming (AFB), wireless sensor networks (WSN), scattering, beampattern, cost and power efficiencies, overhead.

## I. INTRODUCTION

The potential of beamforming to improve the communication range and reliability and the energy efficiency of wireless sensor networks (WSNs) is now well understood in the literature [1]-[14]. Using this technique, a communication link between distant transceivers is established through  $K$  WSN nodes that simultaneously transmit weighted versions of their received signals. These amplify-and-forward (AF) beamforming (AFB) weights are properly designed to ensure a constructive combination at the desired direction of the nodes' radiated energies. When the total transmit power is fixed, AFB can achieve up to  $K$ -fold gain in the received power at the intended direction [9], [13], [15]. As such, not only the communication range is substantially extended, but also each

node decreases its transmission power inversely proportional to  $K$ , thereby preserving their limited energy resources.

The AFB has aroused an increased interest due to its practical benefits. [2] has introduced the AFB concept and analyzed the behavior of its beampattern when nodes are uniformly distributed. Beampattern characteristics have been also evaluated in [4] when the nodes are Gaussian distributed. [5] analyzed the beampattern properties for several node distributions, [6] and [8] have, respectively, proposed nodes selection schemes aiming to achieve narrower mainbeam and minimum sidelobe effects. [9] has studied the robustness of AFB against the nodes asynchrony and [10] has proposed synchronization methods suitable for WSNs. [12] and [13] have summarized the different beamforming techniques and their required synchronization approaches, respectively.

Despite their valuable contributions, all these works assume single-ray (i.e., monochromatic) channels that are very often invalid in real-world applications due to the presence of scattering. Characterized by its angular spread (AS), such a phenomenon replicates the transmit signal along multiple rays from different angles, thereby forming a multi-ray (i.e., polychromatic) channel [16]-[24]. [21] has studied the scattering effect on monochromatic AFB whose design neglects such a phenomenon to show that its performance significantly deteriorates when AS increases. Aiming to address this issue, [22] and [23] have developed bichromatic AFBs which rely on an efficient two-ray channel approximation valid only for low AS. It has been shown that their performances are almost optimal in lightly- to moderately- scattered environments where AS is small. However, they deteriorate in highly-scattered environments where AS is large, more so in the presence of interference.

In order to cope with real-world conditions, many works adopted under different expressions “optimal”<sup>1</sup> amplify-and-forward beamforming (OB) since it is the sole design able to properly handle both interference and scattering [22]-[30]. Unfortunately, each OB weight depends not only on the node's channel state information (CSI)s, but also on the other nodes' CSI)s. Since WSN nodes are autonomous and, hence, do not a priori have access to the other nodes' CSI)s, they have to exchange the latter to be able to compute their respective

Work supported by the DG and CREATE PERSWADE <www.createperswade.ca> Programs of NSERC and a Discovery Accelerator Supplement Award from NSERC.

<sup>1</sup>In the sense that they assume perfect knowledge of both the desired and interfering channels or some quantized approximations thereof.

weights. This results in both huge data overhead and node power depletion, making OB unsuitable for WSNs. This critical impediment motivates us to design a new AFB technique able to approach OB performance at very low overhead and power costs.

In this paper, OB is considered to establish a communication through a WSN of  $K$  sensor nodes from a source to a receiver in the presence of both scattering and interference. All sources send their data to the WSN during the first time slot while the nodes forward a properly weighted version of their received signals during the second slot. These zero-forcing beamforming (ZFB) weights are properly selected to maximize the desired power while completely canceling the interference signals. We show, however, that they depend on information locally unavailable at each node, making them unsuitable for WSNs from the prohibitive data exchange overhead and power depletion they would otherwise require. To address this issue, we exploit the asymptotic expression at large  $K$  of the ZFB weights that is locally computable at every node and, further, well-approximates their original counterparts. The performance of the resulting new distributed ZFB (DZFB) version is analyzed and compared to ZFB and both monochromatic and bichromatic AFBs to highlight its significant performance advantages over all benchmarks.

*Notation:* Uppercase and lowercase bold letters denote matrices and column vectors, respectively.  $[\cdot]_{il}$  and  $[\cdot]_i$  are the  $(i, l)$ -th entry of a matrix and  $i$ -th entry of a vector, respectively.  $(\cdot)^*$ ,  $(\cdot)^T$ , and  $(\cdot)^H$  denote the complex conjugate, the transpose, and the Hermitian transpose, respectively.  $\|\cdot\|$  is the 2-norm of a vector,  $|\cdot|$  is the absolute value, and  $\odot$  is the element-wise product.  $J_n(\cdot)$  and  $I_n(\cdot)$  stand for the first-kind Bessel function and the modified Bessel function of order  $n$ , respectively.

## II. SYSTEM MODEL

As illustrated in Fig. 1, we consider a WSN of  $K$  sensor nodes, each equipped with a single antenna, a receiver  $Rx$ , and  $M$  sources including a desired source and  $M_I = M - 1$  interfering ones. The nodes are assumed to be uniformly distributed over a disc of radius  $R$ . It is also assumed that the channel from the desired source to the destination experiences severe pathloss attenuation making the latter unable to communicate directly, i.e., without relaying from the  $K$  sensor nodes. Let  $(A_m, \phi_m)$  and  $(r_k, \psi_k)$  denote the polar coordinates of the  $m$ -th source and the  $k$ -th node, respectively. Without any loss of generality,  $(A_1, \phi_1 = 0)$  is assumed to be the location of the desired source. We also assume that the  $m$ -th source is located in the far-field region and, hence,  $A_m \gg R$ .

The following assumptions are also adopted in this work:

(i) Due to the presence of a given number of scatterers,  $L_m$  rays are generated from the  $m$ -th source signal to form a polychromatic channel. The  $l$ -th ray has a complex amplitude  $\alpha_{l,m}$  and an angle deviation  $\theta_{l,m}$  from the nominal direction  $\phi_m$ . The  $\alpha_{l,m}$ s are independent and identically distributed (i.i.d) zero-mean random variables (RV)s with variance  $1/L_m$ . The  $\theta_{l,m}$ s are i.i.d. zero-mean RV with a symmetric probability density function (pdf)  $p_m(\theta)$  and variance  $\sigma_m^2$ . The latters

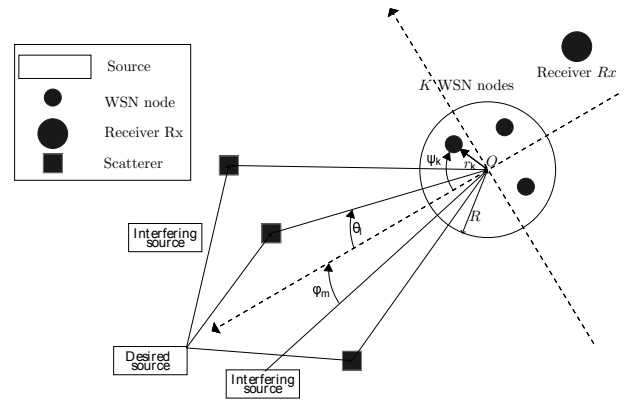


Fig. 1. System model.

are known as scattering distribution and angular spread (AS), respectively. All  $\theta_{l,m}$ s and  $\alpha_{l,m}$ s are mutually independent.

(ii) The  $k$ -th node's forward channel (i.e., from this node to the receiver)  $[\mathbf{f}]_k$  is a circular complex Gaussian zero-mean RV with unit-variance and, hence, its magnitude follows a Rayleigh distribution whose parameter  $\frac{1}{\sqrt{2}}$ .

(iii) Noises at both the receiver and nodes are zero-mean Gaussian RVs with variances  $\sigma_n^2$  and  $\sigma_v^2$ , respectively. All sources' signals are narrow band zero-mean RVs statistically independent from noises and channels.

(iv) Each node has perfect knowledge of its own location and forward channel, the wavelength  $\lambda$ , and the total number of WSN nodes  $K$ . However, it is not privy to other nodes information (i.e., locations and channels).

Note that (i), which is frequently adopted in the context of scattering environments, is due to both the sources' far-field location and the presence of scatterers [19]-[24]. In such a case, channels experience large-scale fading where the pathloss and scattering phenomenon are predominant. In turns, (ii) is due to the short distance between  $Rx$  and nodes, making their channels experience small scale-fading often modeled as Rayleigh distribution [15] [29] [31] [32].

Assumption (i) along with  $A_m \gg R$  implies that the backward channel  $[\mathbf{g}_m]_k$  from the  $m$ -th source to the  $k$ -th node is

$$[\mathbf{g}_m]_k = \sum_{l=1}^{L_m} \alpha_{l,m} e^{-j \frac{2\pi}{\lambda} r_k \cos(\phi_m + \theta_{l,m} - \psi_k)}. \quad (1)$$

Please note that (1) generalizes the well-known steering vector in the array-processing literature [2]-[6], [16], [23]. Indeed, (1) reduces to

$$[\mathbf{g}_m^{(1)}]_k = e^{-j(2\pi/\lambda)r_k \cos(\phi_m - \psi_k)}, \quad (2)$$

in scattering-free environments where  $\sigma_m = 0$ . Please note that  $[\mathbf{g}_m^{(1)}]_k$  is the monochromatic single-ray channel adopted when designing the monochromatic AFB (MB) technique.

## III. ZERO-FORCING AF BEAMFORMER

The desired source communicates with  $Rx$  over a dual-hop transmission. The  $m$ -th source also sends its signal  $s_m$  to the

WSN during the first time slot. The received signal vector  $\mathbf{y}$  at the WSN nodes is

$$\mathbf{y} = \mathbf{g}_1 s_1 + \mathbf{G}_1 \mathbf{s}_1 + \mathbf{v}, \quad (3)$$

where  $\mathbf{G}_1 = [\mathbf{g}_2 \dots \mathbf{g}_M]$ ,  $\mathbf{s}_1 = [s_2 \dots s_M]^T$ , and  $\mathbf{v}$  denotes the noise vector at the nodes. During the second time slot, the  $k$ -th node forwards its received signal after multiplying it with the complex conjugate of the beamforming weight  $w_k$ . Hence,  $R_x$  receives

$$\begin{aligned} r &= \mathbf{f}^T (\mathbf{w}^* \odot \mathbf{y}) + n \\ &= \mathbf{w}^H (\mathbf{f} \odot (\mathbf{g}_1 s_1 + \mathbf{G}_1 \mathbf{s}_1) + \mathbf{f} \odot \mathbf{v}) + n \\ &= s_1 \mathbf{w}^H \mathbf{h}_1 + \mathbf{w}^H \mathbf{H}_1 \mathbf{s}_1 + \mathbf{w}^H (\mathbf{f} \odot \mathbf{v}) + n, \end{aligned} \quad (4)$$

where  $n$  is the receiver's noise,  $\mathbf{h}_1 = \mathbf{f} \odot \mathbf{g}_1$ , and  $\mathbf{H}_1 = [\mathbf{f} \odot \mathbf{g}_2 \dots \mathbf{f} \odot \mathbf{g}_M]$  is a matrix of dimension  $(K, M)$ . Various design approaches may be adopted to derive the beamforming weights. Among them is the zero-forcing (ZF) approach that puts nulls at the interfering directions while ensuring a unit response at the desired source direction. Mathematically, the ZF beamforming (ZFB) vector  $\mathbf{w}_{ZF}$  must satisfy the following equations:

$$\mathbf{w}_{ZF}^H \mathbf{H}_1 = 0, \quad (5)$$

$$\mathbf{w}_{ZF}^H \mathbf{h}_1 = 1. \quad (6)$$

It can be easily shown that  $\mathbf{w}_{ZF}$  is given by

$$\mathbf{w}_{ZF} = \frac{(\mathbf{h}_1 - \mathbf{H}_1 (\mathbf{H}_1^H \mathbf{H}_1)^{-1} \mathbf{H}_1^H \mathbf{h}_1)}{(\|\mathbf{h}_1\|^2 - \mathbf{h}_1^H \mathbf{H}_1 (\mathbf{H}_1^H \mathbf{H}_1)^{-1} \mathbf{H}_1^H \mathbf{h}_1)}. \quad (7)$$

Please note in order to derive  $\mathbf{w}_{ZF}$ , one need to compute the inverse of  $\mathbf{H}_1$  [12]. Since  $K$  is typically much larger than  $M$  especially in WSN applications,  $\mathbf{H}_1$  is not a square matrix and, hence, its inverse does not exist. Nevertheless, according to its definition,  $\mathbf{H}_1$  has linearly independent columns, making thereby the square matrix  $(\mathbf{H}_1^H \mathbf{H}_1)$  invertible. Consequently, one may resort to the pseudo inverse  $(\mathbf{H}_1^H \mathbf{H}_1)^{-1} \mathbf{H}_1^H$  as in 7.

In order to implement  $\mathbf{w}_{ZF}$ , the  $k$ -th node must then be able to compute its corresponding weight

$$\begin{aligned} [\mathbf{w}_{ZF}]_k &= \left( [\mathbf{h}_1]_k - \sum_{m=1}^M [\mathbf{H}_1]_{km} \left[ (\mathbf{H}_1^H \mathbf{H}_1)^{-1} \mathbf{H}_1^H \mathbf{h}_1 \right]_m \right) \\ &\times \left( \sum_{k=1}^K \left( \left[ \mathbf{h}_1 \right]_k \right)^2 - \sum_{m=1}^M [\mathbf{H}_1]_{km} \left[ (\mathbf{H}_1^H \mathbf{H}_1)^{-1} \mathbf{H}_1^H \mathbf{h}_1 \right]_m \right)^{-1}. \end{aligned} \quad (8)$$

A straightforward inspection of (8) reveals that  $[\mathbf{w}_{ZF}]_k$  depends not only on  $[\mathbf{h}_1]_k$ ,  $k = 1, \dots, K$ , but also  $\left[ (\mathbf{H}_1^H \mathbf{H}_1)^{-1} \mathbf{H}_1^H \mathbf{h}_1 \right]_m$ ,  $m = 2, \dots, M$  both dependent on the coordinates and channels of all collaborating WSN nodes. As the latters are completely independent and autonomous, they would need to exchange their locally available information with each other in order to compute their weights, thereby resulting in a prohibitive overhead that can hinder both WSN spectral and power efficiencies. Consequently, the conventional ZFB in (7) is unsuitable for implementation in WSNs.

#### IV. PROPOSED AF BEAMFORMER

To address the aforementioned critical issue, we propose in this work to substitute  $(\mathbf{H}_1^H \mathbf{H}_1)^{-1} \mathbf{H}_1^H \mathbf{h}_1$  and  $\|\mathbf{h}_1\|^2/K$  in  $\mathbf{w}_{ZF}$  with their asymptotic approximations at large  $K$  given as

$$\begin{aligned} \lim_{K \rightarrow \infty} (\mathbf{H}_1^H \mathbf{H}_1)^{-1} \mathbf{H}_1^H \mathbf{h}_1 &= \left( \lim_{K \rightarrow \infty} \frac{\mathbf{H}_1^H \mathbf{H}_1}{K} \right)^{-1} \lim_{K \rightarrow \infty} \frac{\mathbf{H}_1^H \mathbf{h}_1}{K} \\ &= \mathbf{\Pi}^{-1} \boldsymbol{\beta}, \end{aligned} \quad (9)$$

and

$$\lim_{K \rightarrow \infty} \frac{\|\mathbf{h}_1\|^2}{K} = \beta_0, \quad (10)$$

respectively. Actually, this approximation is motivated by the fact that the number of WSN nodes is typically large. In what follows, we will prove that both  $\mathbf{\Pi}$  and  $\boldsymbol{\beta}$  depend on the information locally available at each node, thereby paving the way towards the distributed implementation of ZFB in such networks. Let us first start by  $\mathbf{\Pi}$ . According to the definition of  $\mathbf{H}_1$ , we have for  $p, q = 1, \dots, M$

$$\begin{aligned} [\mathbf{\Pi}]_{pq} &= \lim_{K \rightarrow \infty} \frac{1}{K} [\mathbf{H}_1^H \mathbf{H}_1]_{pq} \\ &= \sum_{l, l'=1}^L \alpha_{l, p+1} \alpha_{l', q+1}^* \lim_{K \rightarrow \infty} \sum_{k=1}^K \frac{|\mathbf{f}[k]|^2}{K} \\ &\times e^{-j \frac{2\pi}{\lambda} r_k (\cos(\phi_{q+1} + \theta_{l, p+1} - \psi_k) - \cos(\phi_{p+1} + \theta_{l', q+1} - \psi_k))}. \end{aligned} \quad (11)$$

Exploiting the strong law of large numbers (LLN), we obtain

$$\begin{aligned} [\mathbf{\Pi}]_{pq} &= \sum_{l, l'=1}^L \alpha_{l, p+1} \alpha_{l', q+1}^* \mathbb{E}_{r_k, \psi_k, \mathbf{f}[k]} \left\{ |\mathbf{f}[k]|^2 \right. \\ &\times e^{-j \frac{2\pi}{\lambda} r_k (\cos(\phi_{q+1} + \theta_{l, p+1} - \psi_k) - \cos(\phi_{p+1} + \theta_{l', q+1} - \psi_k))} \left. \right\}, \end{aligned} \quad (12)$$

where  $\mathbb{E}_{r_k, \psi_k, \mathbf{f}[k]}$  stands for the expectation taken with respect to the random variables  $r_k$ s,  $\psi_k$ s,  $\mathbf{f}[k]$ s. Since these RVs are independent and, according to assumption (ii),  $\mathbb{E}\{|\mathbf{f}[k]|^2\} = 1$ , the expectation in (12) could be expressed as (13) where  $z_k = \frac{r_k}{R} \sin\left(\frac{\phi_{p+1} + \phi_{q+1} + \theta_{l, p+1} + \theta_{l', q+1}}{2} - \psi_k\right)$  and  $f_{z_k}(z)$  is its pdf. In order to compute the latter, one must have prior knowledge of the WSN nodes' distribution. Please note here that such information could be either easily integrated in nodes' memories prior to deployment or broadcasted by the receiver at negligible overhead and power costs. Since the WSN nodes are uniformly distributed over a disc of radius  $R$ , one can easily show that  $f_{z_k}(z) = \frac{2}{\pi} \sqrt{1-z^2}$ ,  $z \in [-1, 1]$  [2]. Exploiting the power series expansion of the exponential function in (13), we obtain (14) as shown on the top of the next page where

$$\Delta(\phi) = 2 \frac{J_1\left(4\pi \frac{R}{\lambda} \sin(\phi/2)\right)}{4\pi \frac{R}{\lambda} \sin(\phi/2)}. \quad (15)$$

Please note in the third line of (14) that we use the power series expansion of the Bessel function given by  $J_n(x) = \sum_{p=0}^{+\infty} \frac{(-1)^p}{p!(n+p)!} \left(\frac{x}{2}\right)^{2p+n}$ . It follows from (14) and (15) that  $\mathbf{\Pi}$

$$\mathbb{E}_{r_k, \psi_k} \left\{ e^{-j \frac{4\pi R}{\lambda} \sin\left(\frac{\phi_{p+1} - \phi_{q+1} + \theta_{l,p+1} - \theta_{l',q+1}}{2}\right)} \frac{r_k}{R} \sin\left(\frac{\phi_{p+1} + \phi_{q+1} + \theta_{l,p+1} + \theta_{l',q+1}}{2} - \psi_k\right) \right\} = \int_{-1}^1 e^{-j \frac{4\pi R}{\lambda} \sin\left(\frac{\phi_{p+1} - \phi_{q+1} + \theta_{l,p+1} - \theta_{l',q+1}}{2}\right)} z_k f_{z_k}(z) dz, \quad (13)$$

$$\begin{aligned} [\mathbf{\Pi}]_{pq} &= \sum_{l, l'=1}^L \alpha_{l,p+1} \alpha_{l',q+1}^* \left( \sum_{p=0}^{+\infty} \frac{(4\pi \frac{R}{\lambda})^p \sin^p\left(\frac{\phi_{p+1} - \phi_{q+1} + \theta_{l,p+1} - \theta_{l',q+1}}{2}\right)}{p!} (-j)^p \int_{-1}^1 z_k^p \frac{2}{\pi} \sqrt{1-z^2} dz \right) \\ &= \sum_{l, l'=1}^L \alpha_{l,p+1} \alpha_{l',q+1}^* \left( \sum_{p=0}^{+\infty} \frac{(4\pi \frac{R}{\lambda})^{2p} \sin^{2p}\left(\frac{\phi_{p+1} - \phi_{q+1} + \theta_{l,p+1} - \theta_{l',q+1}}{2}\right) (-1)^p}{2^{2p} p! (p+1)!} \right) \\ &= \sum_{l, l'=1}^L \alpha_{l,p+1} \alpha_{l',q+1}^* \Delta(\phi_{p+1} - \phi_{q+1} + \theta_{l,p+1} - \theta_{l',q+1}), \end{aligned} \quad (14)$$

depends solely on information locally available at every collaborating node and, hence, is locally computable. Following the above steps, one can also obtain for  $p = 1, \dots, M_I$

$$\begin{aligned} [\boldsymbol{\beta}]_p &= \lim_{K \rightarrow \infty} \frac{[\mathbf{H}_I^H \mathbf{h}_1]_p}{K} \\ &= \sum_{l, l'=1}^L \alpha_{l,p+1} \alpha_{l',1}^* \Delta(\phi_{p+1} + \theta_{l,p+1} - \theta_{l',1}), \end{aligned} \quad (16)$$

and

$$\boldsymbol{\beta}_0 = \sum_{l, l'=1}^L \alpha_{l,1} \alpha_{l',1}^* \Delta(\theta_{l',1} - \theta_{l,1}). \quad (17)$$

As could be observed from (16) and (17),  $\boldsymbol{\beta}$  and  $\boldsymbol{\beta}_0$  are also independent of any information unavailable at every node, making them locally computable as well. Using (14), (16), and (17), we introduce our proposed DZFB vector

$$\mathbf{w}_P = \frac{(\mathbf{h}_1 - \mathbf{H}_I \boldsymbol{\Pi}^{-1} \boldsymbol{\beta})}{K (\boldsymbol{\beta}_0 - \boldsymbol{\beta}^H \boldsymbol{\Pi}^{-1} \boldsymbol{\beta})}. \quad (18)$$

If  $\mathbf{w}_P$  is implemented in lieu of  $\mathbf{w}_{ZF}$ , the  $k$ -th node would require  $[\mathbf{h}_1]_k$  and  $[\mathbf{H}_I]_{km}, m = 2, \dots, M$  (i.e., its own channels) as well as  $\boldsymbol{\beta}_0, \boldsymbol{\Pi}^{-1}$ , and  $\boldsymbol{\beta}$ , in order to derive its corresponding beamforming weight

$$\begin{aligned} [\mathbf{w}_P]_k &= \frac{1}{K} \left( [\mathbf{h}_1]_k - \sum_{m=1}^M [\mathbf{H}_I]_{km} [\boldsymbol{\Pi}^{-1} \boldsymbol{\beta}]_m \right) \\ &\times \left( \boldsymbol{\beta}_0 - \sum_{m=1}^M [\boldsymbol{\beta}^H]_m [\boldsymbol{\Pi}^{-1} \boldsymbol{\beta}]_m \right)^{-1}. \end{aligned} \quad (19)$$

According to (14)-(17), all these entities depend solely on information locally available and/or obtainable at the  $k$ -th node. Therefore, the computation of  $[\mathbf{w}_P]_k$  does not require any information exchange between nodes, thereby lending itself to a distributed implementation over WSNs, that is in sharp contrast to  $[\mathbf{w}_{ZF}]_k$  in (8). By substantially reducing the overhead, the new DZFB dramatically improves both WSN spectral and power efficiencies.

## V. ACHIEVED BEAMPATTERN CHARACTERISTICS

In order to verify the efficiency of the proposed distributed DZFB and its compliance with the conditions (5) and (6), we analyze in this section the characteristics of its achieved beampattern. The latter is nothing but the received power at  $Rx$  from any source located at  $\phi_*$  and hence is defined for any AFB vector  $\mathbf{w}$  as

$$P_{\mathbf{w}}(\phi_*) = |\mathbf{w}^H \mathbf{h}_m|^2. \quad (20)$$

It follows from (20) that  $P_{\mathbf{w}_P}(\phi_*)$  is a complex combination of several random variables, making its analysis a tedious task. In this work, we propose to study instead the behavior of the average beampattern  $\bar{P}_{\mathbf{w}_P}(\phi_*) = \mathbb{E}_{r_k, \psi_k, [\mathbf{F}]_k} \left\{ |\mathbf{w}_P^H \mathbf{h}_m|^2 \right\}$  where the expectation is taken over all nodes' forward channels and positions.

The main result of this section is given in the following theorem:

*Theorem 1:* For any given  $p_m(\theta)$  and  $\sigma_m, m = 1, \dots, M$ ,  $\bar{P}_{\mathbf{w}_P}(\phi_*)$  can be expressed as

$$\begin{aligned} \bar{P}_{\mathbf{w}_P}(\phi_*) &= (\boldsymbol{\beta}_0 - \boldsymbol{\beta}^H \boldsymbol{\Pi}^{-1} \boldsymbol{\beta})^{-2} \left( \frac{1}{K} \left( \Sigma_0(\phi_*) \right. \right. \\ &\quad \left. \left. - 2\text{Re}(\Sigma_2^H(\phi_*) \boldsymbol{\Pi}^{-1} \boldsymbol{\beta}) + \boldsymbol{\beta}^H \boldsymbol{\Pi}^{-1} \Sigma_3(\phi_*) \boldsymbol{\Pi}^{-1} \boldsymbol{\beta} \right) \right. \\ &\quad \left. + \left( 1 - \frac{1}{K} \right) \left| \Sigma_1(\phi_*) - \Sigma_4^H(\phi_*) \boldsymbol{\Pi}^{-1} \boldsymbol{\beta} \right|^2 \right), \end{aligned} \quad (21)$$

where the scalars  $\Sigma_0$  and  $\Sigma_1$  as well the vectors  $\Sigma_2, \Sigma_3$ , and  $\Sigma_4$  are complex functions of the sources' directions and their angular deviations.

*Proof:* See Appendix A.

It follows from (21) that the desired power  $\bar{P}_{\mathbf{w}_P}(\phi_1 = 0)$  boils down for large  $K$  to

$$\bar{P}_{\mathbf{w}_P}(0) = \left( \frac{|\Sigma_1(0) - \Sigma_4^H(0) \boldsymbol{\Pi}^{-1} \boldsymbol{\beta}|}{(\boldsymbol{\beta}_0 - \boldsymbol{\beta}^H \boldsymbol{\Pi}^{-1} \boldsymbol{\beta})} \right)^2. \quad (22)$$

It can be inferred from the definitions of  $\Sigma_1(\phi_m)$  and  $\Sigma_4(\phi_m)$  that they reduce for  $\phi_m = \phi_1 = 0$  to  $\beta_0$  and  $\beta$ , respectively. Consequently, from (22),  $\bar{P}_{\mathbf{w}_P}(0) = 1$  when  $K$  is large enough. This implies that the proposed DZFB guarantees a unit received power response at the desired direction, thereby satisfying at large  $K$  the condition in (5) as its conventional ZFB counterpart which is, however, unsuitable for a distributed implementation over WSNs. Simulations in Section VII will prove that  $\bar{P}_{\mathbf{w}_P}(0)$  exhibits for small  $K$  only a slight deterioration. Actually, this loss is nothing but the cost of adopting the asymptotic approximation at large  $K$  when designing  $\mathbf{w}_P$  in Section IV. Nevertheless,  $\bar{P}_{\mathbf{w}_P}(0)$  increases rapidly with  $K$  and reaches 1 for  $K$  in the range of 10.

Let us now derive the power received from the interfering sources. According to the definition of  $\Sigma_4^H(\phi_m)$  in Appendix A, we have for  $m = 2, \dots, M$

$$\begin{aligned} [\Sigma_4(\phi_m)]_p &= \sum_{l,l'=1}^L \alpha_{l,m} \alpha_{l',p+1}^* \Delta(\theta_{l,m} - \theta_{l',p+1} + \phi_m - \phi_{p+1}) \\ &= [\mathbf{\Pi}]_{(m-1)p}. \end{aligned} \quad (23)$$

This implies that  $\Sigma_4(\phi_m) = e_m \mathbf{\Pi}$  where  $e_m$  is the vector having 1 in its  $m$ -th entry and zeros elsewhere. Exploiting this propriety, one can easily prove that

$$\Sigma_1(\phi_m) = \Sigma_4^H(\phi_m) \mathbf{\Pi}^{-1} \beta. \quad (24)$$

It follows from (21) and (24) that the  $m$ -th interference power is given by

$$\begin{aligned} \bar{P}_{\mathbf{w}_P}(\phi_m) &= \frac{1}{K \left( \beta_0 - \beta^H \mathbf{\Pi}^{-1} \beta \right)^2} \left( \Sigma_0(\phi_m) \right. \\ &\quad \left. - 2\text{Re} \left( \Sigma_2^H(\phi_m) \mathbf{\Pi}^{-1} \beta \right) + \beta^H \mathbf{\Pi}^{-1} \Sigma_3(\phi_m) \mathbf{\Pi}^{-1} \beta \right). \end{aligned} \quad (25)$$

Despite its efficiency, our proposed technique does not totally suppress the interference sources, in contrast to conventional ZFB that can perfectly implement the condition (5) while being, however, unsuitable for a distributed implementation over WSNs. Actually, this is again the cost of adopting the asymptotic approximation approach introduced in Section IV when designing  $\mathbf{w}_P$ . Nevertheless, according to (25), the proposed DZFB is able to linearly reduce the powers of all interfering sources by factor  $K$  and, hence, cancel them, when the number of collaborating nodes is large enough.

All these observations verify that the average beampattern achieved by the proposed DZFB has a main lobe peak at the desired source direction and  $(M-1)$  minima at the interfering ones. As  $K$  grows large, the peak's and minima's values approach 1 and 0, respectively, thereby satisfying (5) and (6) as its ZFB counterpart which is, however, unsuitable for a distributed implementation over WSNs.

In the sequel, we compare the performance of our proposed technique with the existing distributed AFB benchmarks.

## VI. PERFORMANCE COMPARISON WITH DISTRIBUTED AFB BENCHMARKS

So far, only two distributed AFB techniques exist: the monochromatic AFB  $\mathbf{w}_M$  which ignores scattering to assume

a single-ray channel [2] [4] [8] [31] and the bichromatic AFB  $\mathbf{w}_B$  whose design relies on a polychromatic channel's approximation by two chromatics at  $\pm\sigma_\theta$  when the latter is relatively small [22] [23]. It can be easily shown that  $\mathbf{w}_M$  is given by

$$\mathbf{w}_M = \frac{(\mathbf{h}_{M,1} - \mathbf{H}_{M,I} \mathbf{\Pi}_M^{-1} \beta_M)}{K \left( 1 - \beta_M^H \mathbf{\Pi}_M^{-1} \beta_M \right)}, \quad (26)$$

where  $\mathbf{h}_{M,m} = \mathbf{f} \odot \mathbf{g}_m^{(1)}$ ,  $\mathbf{H}_{M,I}^H = [\mathbf{f} \odot \mathbf{g}_2^{(1)} \dots \odot \mathbf{g}_M^{(1)}]$ ,  $[\mathbf{\Pi}_M]_{ij} = \Delta(\phi_{i+1} - \phi_{j+1})$ , and  $[\beta_M]_i = \Delta(\phi_{i+1})$ . Whereas,  $\mathbf{w}_B$  is given by

$$\mathbf{w}_B = \frac{(\mathbf{h}_{B,1} - \mathbf{H}_{B,I} \mathbf{\Pi}_B^{-1} \beta_B)}{K \left( 1 + \Delta(2\sigma_\theta) - \beta_B^H \mathbf{\Pi}_B^{-1} \beta_B \right)}, \quad (27)$$

where  $\mathbf{h}_{B,m} = \mathbf{f} \odot (e^{-j(2\pi/\lambda)r_k \cos(\phi_m + \sigma_m - \psi_k)} + e^{-j(2\pi/\lambda)r_k \cos(\phi_m - \sigma_m - \psi_k)})$ ,  $\mathbf{H}_{B,I}^H = [\mathbf{h}_{B,2} \dots \mathbf{h}_{B,M}]$ ,  $[\mathbf{\Pi}_B]_{ij} = \Delta(\tilde{\phi}_{i+1} - \tilde{\phi}_{j+1})$ , and  $[\beta_B]_i = \Delta(\tilde{\phi}_1 - \tilde{\phi}_{i+1})$  with  $\tilde{\phi}_i = \phi_{i/2} - \sigma_{i/2}$  if  $i$  is even and  $\tilde{\phi}_i = \phi_{(i-1)/2+1} + \sigma_{(i-1)/2+1}$  if  $i$  is odd. It follows from (26) and (27) that both  $\mathbf{w}_M$  and  $\mathbf{w}_B$  depend on the information commonly available at each node and, hence, lend themselves to a distributed implementation over WSNs.

In order to compare our proposed distributed AFB with its monochromatic and bichromatic counterparts, we need a performance metric that captures each technique's compliance with the design conditions (5) and (6). For the sake of tractability, we propose in this paper to adopt the achieved average-signal-to-average-interference-plus-noise ratio (ASAINR) defined for any  $\mathbf{w}$  as  $\gamma_{\mathbf{w}} = \bar{P}_{\mathbf{w}}(0) / (\bar{P}_{\mathbf{w}}(\phi_{m \neq 1}) + \bar{N}_{\mathbf{w}})$  where  $\bar{N}_{\mathbf{w}}$  is the average noise power incurred by  $\mathbf{w}$ . To this end, one should first derive the equations of the achieved average beampattern using  $\mathbf{w}_M$  and  $\mathbf{w}_B$ . To do so, we introduce the following theorem:

*Theorem 2:* For any given  $p_m(\theta)$  and  $\sigma_m$ ,  $m = 1, \dots, M$ ,  $\bar{P}_{\mathbf{w}_B}(\phi_*)$  can be expressed as

$$\bar{P}_{\mathbf{w}_B}(\phi_*) = \frac{\frac{2}{K} + \left( 4 \left( 1 - \frac{1}{K} \right) \frac{\Psi_B(\phi_*)}{(1 + \Delta(2\sigma_1) - \beta_B^H \mathbf{\Pi}_B^{-1} \beta_B)} \right)}{\left( 1 + \Delta(2\sigma_1) - \beta_B^H \mathbf{\Pi}_B^{-1} \beta_B \right)}, \quad (28)$$

where

$$\begin{aligned} \Psi_B(\phi_*) &= \int_{\Theta_*} \frac{p_*(\theta)}{2} \left( \Delta(\phi_* + \theta + \sigma_1) + \Delta(\phi_* + \theta - \sigma_1) \right. \\ &\quad \left. - 2\tau_B(\phi_* + \theta)^T \mathbf{\Pi}_B^{-1} \beta_B \right)^2 d\theta, \end{aligned} \quad (29)$$

with  $[\tau_B(\theta)]_m = (1/2)\Delta(\theta - \tilde{\phi}_{m+2})$  if  $\theta \neq \tilde{\phi}_{m+2}$  and  $[\tau_B(\theta)]_m = 1/2$  otherwise, and  $\Theta_*$  is the span of the pdf  $p_*(\theta)$  over which the integral is calculated.<sup>2</sup>

<sup>2</sup>In the Gaussian and Uniform distribution cases,  $\Theta_* = [-\text{inf}, +\text{inf}]$  and  $\Theta_* = [-\sqrt{3}\sigma_\theta, +\sqrt{3}\sigma_\theta]$ , respectively.

In turn  $\bar{P}_{\mathbf{w}_M}(\phi_*)$  is given by

$$\bar{P}_{\mathbf{w}_M}(\phi_*) = \frac{\frac{1}{K} + \left(4 \left(1 - \frac{1}{K}\right) \frac{\Psi_M(\phi_*)}{(1 - 2\beta_M^T \mathbf{\Pi}_M^{-1} \beta_M)}\right)}{\left(1 - 2\beta_M^T \mathbf{\Pi}_M^{-1} \beta_M\right)}, \quad (30)$$

where

$$\Psi_M(\phi_*) = \int_{\Theta_*} p_*(\theta) \left(\Delta(\phi_* + \theta) - 2\tau_M(\phi_* + \theta)^T \mathbf{\Pi}_B^{-1} \beta_B\right)^2 d\theta, \quad (31)$$

with  $[\tau_M(\theta)]_m = (1/2)\Delta(\theta - \phi_{m+1})$ .

*Proof:* See Appendix B.

### A. DZFB Gains Against Bichromatic AFB

It follows from (21) and (28) that the ASAINR gain achieved by the proposed AFB over its bichromatic counterpart reduces for large  $K$  to

$$\zeta_B = \frac{4 \left(1 + \Delta(2\sigma_1) - \beta_B^T \mathbf{\Pi}_B^{-1} \beta_B\right)^2}{\Psi_B(0)}, \quad (32)$$

where  $\zeta_B = \gamma_{\mathbf{w}_P}/\gamma_{\mathbf{w}_B}$ . Exploiting the fact that  $\Delta(x) \rightarrow 1$  when  $x \rightarrow 0$ , one can easily prove from (32) that  $\gamma_{\mathbf{w}_P} = \gamma_{\mathbf{w}_B}$  if  $\sigma_m = 0, m = 1, \dots, M$  (i.e., there is no scattering). This is hardly surprising since  $\mathbf{w}_P$  boils down to  $\mathbf{w}_B$  in such condition. On the other hand, when  $\sigma_m, m = 2, \dots, M$  are relatively small (i.e., in lightly- to moderately-scattered environments), it can be shown that  $\Psi_B(0) \simeq 1$  and  $\beta_B^T \mathbf{\Pi}_B^{-1} \beta_B \ll 1$  if all sources are sufficiently far apart by satisfying [2], [23]

$$\sin(\phi_m - \phi_n) \gg \frac{3\lambda}{16\pi}, m \neq n. \quad (33)$$

Therefore,  $\gamma_{\mathbf{w}_P} \simeq \gamma_{\mathbf{w}_B}$  in lightly- to moderately-scattered environments. This is expected since the bichromatic AFB is able in such environments to achieve the same optimal performance of DZFB. This is due to the validity of the bichromatic channel approximation up to an AS value of around 17 deg. Nevertheless, since  $\Delta(x) \rightarrow 0$  when  $x \rightarrow \text{inf}$ ,  $\gamma_{\mathbf{w}_P} > \gamma_{\mathbf{w}_B}$  when  $\sigma_m$ s grow large. Consequently, DZFB outperforms its bichromatic counterpart in highly-scattered environments. Its achieved ASAINR gain increases with  $\sigma_1$  since  $\Psi_B(0)$  is a decreasing function of the latter.

### B. DZFB Gains Against Monochromatic AFB

From (21) and (28), we have for large  $K$

$$\zeta_M = \frac{4 \left(1 - \beta_M^T \mathbf{\Pi}_M^{-1} \beta_M\right)^2}{\Psi_M(0)}, \quad (34)$$

where  $\zeta_M = \gamma_{\mathbf{w}_P}/\gamma_{\mathbf{w}_M}$ . When the sources are enough distant from each other to satisfy (33), the right hand side (RHS) of (34) reduces to  $4 \left(\int_{\Theta_*} p_*(\theta) \Delta(\theta)^2 d\theta\right)^{-1}$ . Assuming that the scattering distribution is Uniform over  $[-\sqrt{3}\sigma_1, \sqrt{3}\sigma_1]$  (i.e.,

$p(\theta) = 1/2\sqrt{3}\sigma_1$ ), for small  $\sigma_1$  we have

$$\begin{aligned} \zeta_M &\simeq 8\sqrt{3}(\pi R)^2 \sigma_1 \left( \int_{-\sqrt{3}\sigma_1}^{\sqrt{3}\sigma_1} \left( \frac{J_1\left(2\pi \frac{R}{\lambda} \theta\right)}{\theta} \right)^2 d\theta \right)^{-1} \\ &\simeq 8\sqrt{3}\sigma_1 \left( \int_0^{1/2} \frac{{}_2F_3\left(2, \frac{3}{2}; 2, 2, 3, -12\pi^2 \left(\frac{R}{\lambda}\right)^2 \sigma_\theta^2 \theta\right)}{\sqrt{\theta}} d\theta \right)^{-1} \\ &\simeq {}_3F_4\left(\frac{1}{2}, 2, \frac{3}{2}; \frac{3}{2}, 2, 2, 3, -12\pi^2 \left(\frac{R}{\lambda}\right)^2 \sigma_1^2\right)^{-1}, \quad (35) \end{aligned}$$

where  ${}_3F_4\left(\frac{1}{2}, 2, \frac{3}{2}; \frac{3}{2}, 2, 2, 3, -12\pi^2 (R/\lambda)^2 x^2\right)$  is the hypergeometric function. The latter DZFB decreases with  $x$  from its maximum value of 1 obtained at 0. This implies that  $\gamma_{\mathbf{w}_P} = \gamma_{\mathbf{w}_M}$  if  $\sigma_1 = 0$ . This is expected from (18) and (26) since  $\mathbf{w}_P \rightarrow \mathbf{w}_M$  when there is no scattering. On the other hand, it can be inferred from (35) that  $\gamma_{\mathbf{w}_P} > \gamma_{\mathbf{w}_M}$  if  $\sigma_1 \neq 0$ . Therefore, DZFB outperforms its monochromatic vis-a-vis that completely ignores scattering. Besides, its achieved ASAINR gain against the latter increases not only with AS, but also with  $R/\lambda$ .

### C. Insightfulness of the ASINR Metric

This section evaluates the perspicacity of the ASAINR as a metric for faithful and meaningful performance comparisons. To do so, the following theorem establishes a very useful asymptotic relationship between the ASAINR and the more common average SINR (ASINR) metric:

*Theorem 3:* For any  $\mathbf{w} \in \{\mathbf{w}_P, \mathbf{w}_B, \mathbf{w}_M\}$  and any given  $p_m(\theta)$  and  $\sigma_m, m = 1, \dots, M$ , we have

$$\lim_{K \rightarrow \infty} \tilde{\gamma}_{\mathbf{w}} = \lim_{K \rightarrow \infty} \gamma_{\mathbf{w}}, \quad (36)$$

where  $\tilde{\gamma}_{\mathbf{w}}$  denotes the ASINR achieved using  $\mathbf{w}$ .

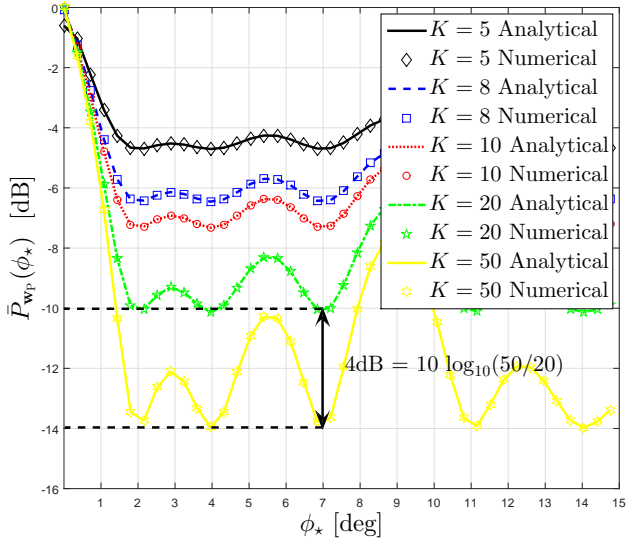
*Proof:* See Appendix C.

The above theorem states that the ASAINR and ASINR are asymptotically equivalent and, hence, we have also  $\lim_{K \rightarrow \infty} \tilde{\zeta}_B = \lim_{K \rightarrow \infty} \zeta_B$  and  $\lim_{K \rightarrow \infty} \tilde{\zeta}_M = \lim_{K \rightarrow \infty} \zeta_M$  where  $\tilde{\zeta}_B$  and  $\tilde{\zeta}_M$  are the ASINR gains of the proposed DZFB against the bichromatic and monochromatic AFBs. Consequently, for large  $K$  the proposed beamformer outperforms also its counterparts in terms of ASINRs well, more so at larger AS values as previously shown in Section VI.

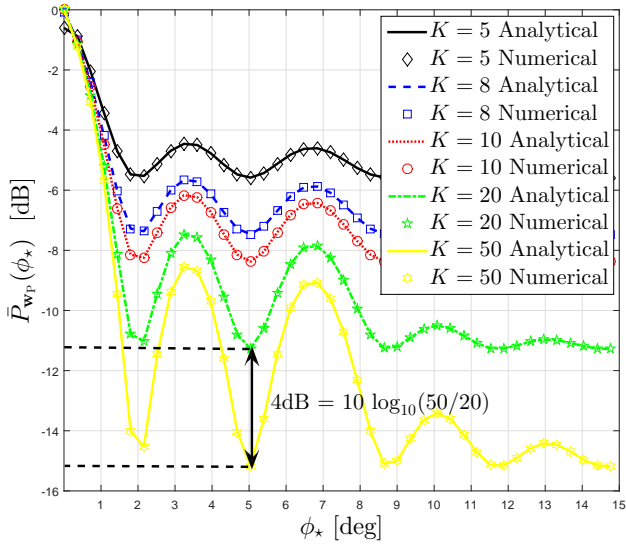
## VII. SIMULATION RESULTS

This section verifies the efficiency of the proposed DZFB using computer simulations. All empirical average quantities are calculated over  $10^6$  random realizations of  $r_k, \psi_k, [\mathbf{f}]_k$  for  $k = 1, \dots, K$  and  $\alpha_{l,m}, \theta_{l,m}$  for  $l = 1, \dots, L_m$ . In all simulations, all sources have the same unit power,  $\sigma_n^2 = \sigma_v^2 = 1$ , and  $L_m = 6$ . We also consider that all rays have equal power  $1/L_m$  (i.e.,  $E\{|\alpha_{l,m}|^2\} = 1/L_m$ ) and  $\theta_{l,m}$ s are uniformly distributed random variables with variance  $\sigma^2$ .

Fig. 2 displays the empirical and analytical (i.e., equation (21)) curves of the average beampattern  $\bar{P}_{\mathbf{w}_P}(\phi_*)$  achieved by DZFB versus  $\phi_*$  for  $\sigma = 35$  deg,  $R/\lambda = 10$ , and different values of  $K$ . We consider in Figs. 2(a) and 2(b) three and



(a)  $(\phi_2, \phi_3, \phi_4) = (2, 4, 7)$  deg



(b)  $(\phi_2, \phi_3) = (2, 5)$  deg

Fig. 2. Empirical and analytical average beampattern  $\bar{P}_{w_P}(\phi_*)$  achieved by DZFB versus  $\phi_*$  for  $\sigma = 35$  deg,  $R/\lambda = 10$ ,  $K = \{5, 8, 10, 20, 50\}$ , and different sets of interfering sources.

two interfering sources at  $(\phi_2, \phi_3, \phi_4) = (2, 4, 7)$  deg and  $(\phi_2, \phi_3) = (2, 5)$  deg, respectively. These figures confirm that the analytical (i.e., equation (21)) and empirical values of  $\bar{P}_{w_P}(\phi_*)$  match perfectly. They also show that the DZFB's average beampattern has a peak at the desired direction (i.e.,  $\phi = 0$ ) and minima at the interfering ones. Furthermore, we observe that  $\bar{P}_{w_P}(0)$  loses a fraction of dB for small  $K$ . As discussed in Section V, this negligible loss results from the asymptotic approximation at large  $K$  assumed in the design of  $w_P$ . Nevertheless, according to Figs. 2(a) and 2(b),  $\bar{P}_{w_P}(0)$  rapidly increases with  $K$  to reach 1 at no more than 10 WSN nodes, thereby satisfying the design condition in (6). Besides, DZFB satisfies also the condition in (5) for relatively large  $K$  as  $\bar{P}_{w_P}(\phi_{m \neq 1})$  substantially decreases with  $K$  to reach  $-11$  and  $-15$  dB at 20 and 50, respectively. And the difference

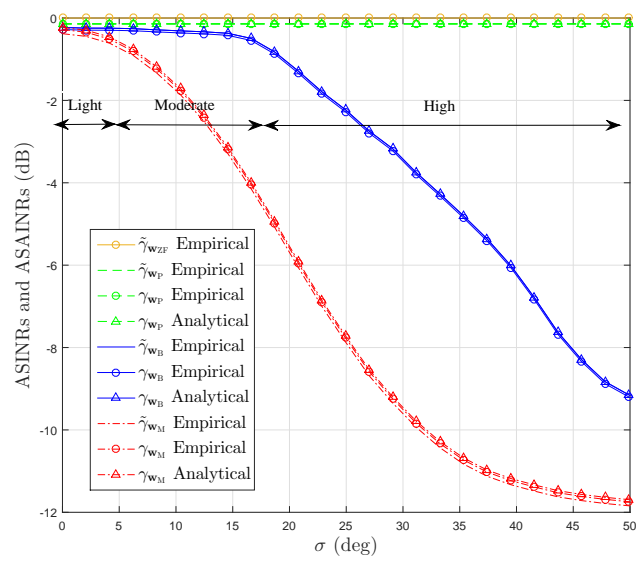


Fig. 3. Empirical ASINRs and ASAINRs achieved by the proposed DZFB and its monochromatic and bichromatic counterparts and their analytical ASAINRs versus  $\sigma$  for  $R/\lambda = 10$  and  $K = 20$ .

of 4 dB (i.e.,  $\log_{10}(50/20)$ ) confirms the linear decrease of interference powers with  $K$  as stated in Section V. The DZFB is clearly able to achieve the optimal performance of its conventional ZFB counterpart whose implementation requires, however, prohibitive overhead and power consumption that makes it unsuitable for distributed implementation over WSNs. All these observations corroborate the analytical results of Section V.

Fig. 3 plots the ASINR and ASAINR achieved by  $w \in \{w_P, w_B, w_M\}$  as well as the ASINR achieved by  $w_{ZF}$  versus the AS  $\sigma$  for  $R/\lambda = 10$  and  $K = 20$ . It shows that the empirical curves match perfectly their analytical counterparts (i.e., equations (21), (28), and (30)), thereby validating the derivations and observations made in Sections V and VI including Theorem 3. Beyond this key verification, we observe from this figure that the ASAINR achieved by the monochromatic AFB starts deteriorating very quickly from optimal performance level as soon as  $\sigma$  increases from 0, making it very sensitive to scattering in interfered environments even if it is light. This is hardly-surprising since  $w_M$  ignores it completely to assume instead a single-ray (i.e., monochromatic) channel that is far from capturing all its polychromatic channel components (especially at moderate or high scattering). Such a channel mismatch becomes even worst when  $\sigma$  increases. On the other hand, DZFB closely approaches the optimal ASINR achieved using  $w_{ZF}$  at any scattering level. Whereas,  $w_B$  approaches the same performance level of  $w_P$  in lightly-to moderately-scattered environments when  $\sigma$  is relatively small. Nevertheless, in highly-scattered environments, its performance substantially deteriorates as the  $\sigma$  grows large (i.e.,  $\sigma \geq 20$  deg). This is hardly surprising since the bichromatic AFB design relies on a two-ray approximation of the polychromatic channel that is only valid at relatively small  $\sigma$ . In highly-scattered environments, the increasing mismatch between the

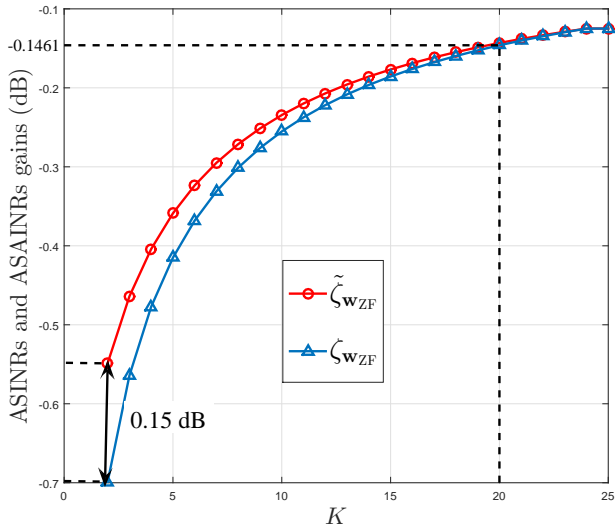


Fig. 4. ASINR and ASAINR gains of the proposed DZFB against its conventional ZFB counterpart versus  $K$  for  $\sigma = 35$  deg and  $R/\lambda = 10$ .

nominal bichromatic channel and the true polychromatic one severely degrades performance.

Fig. 4 displays the ASINR and ASAINR gains achieved by the proposed DZFB against the conventional ZFB benchmark. As could be observed from this figure, for small  $K$  the proposed DZFB loses a fraction of  $dB$  that become more and more negligible as  $K$  increases. At  $K = 20$ , for instance, it loses  $0.1461$   $dB$  which corresponds to as low as 3% loss with respect to the optimal performance achieved by the conventional ZFB. As discussed in Section V, this negligible loss results from the asymptotic approximation at large  $K$  assumed during the design of  $\mathbf{w}_P$  and, hence, it is the price to pay to make the proposed beamformer distributed. On the other hand, according to Fig 4, the ASINR and ASAINR gain curves are indistinguishable for  $K \geq 18$  while exhibiting a small gap of  $0.15$  at  $K = 2$ . This confirms again the relevance of the ASINRs as performance metric and, hence, validates the results in Theorem 3.

Fig. 5 plots the ASINR and ASAINR gains achieved by the proposed DZFB against the monochromatic and bichromatic benchmarks versus  $\sigma$  deg for  $K = 20$  and different values of  $R/\lambda = \{10, 15\}$ . We can check that  $\tilde{\gamma}_{\mathbf{w}_P} = \tilde{\gamma}_{\mathbf{w}_B} = \tilde{\gamma}_{\mathbf{w}_M}$  at  $\sigma = 0$  (i.e., there is no scattering) where we have  $\mathbf{w}_P = \mathbf{w}_B = \mathbf{w}_M$ . In lightly-scattered environments, however, the proposed distributed DZFB outperforms its monochromatic counterpart. The former achieves over the latter an important ASINR gain that increases with  $R/\lambda$  to reach up to 3 dB (i.e.,  $\tilde{\gamma}_{\mathbf{w}_P} = 2\tilde{\gamma}_{\mathbf{w}_M}$ ) for  $R/\lambda = 15$ . In moderately-scattered environments,  $\zeta_M$  increases rapidly with  $\sigma$ , more so at higher  $R/\lambda$ , since  $\mathbf{w}_M$  is severely penalized by much larger channel mismatch. As far as the bichromatic AFB is concerned,  $\zeta_B = 1$  if  $\sigma \leq 17$  deg. In moderately-scattered environments, its ASINR decreases slightly by 2 dB against DZFB at  $\sigma = 20$  deg. In highly-scattered environments, DZFB unambiguously outperforms both its monochromatic and bichromatic coun-

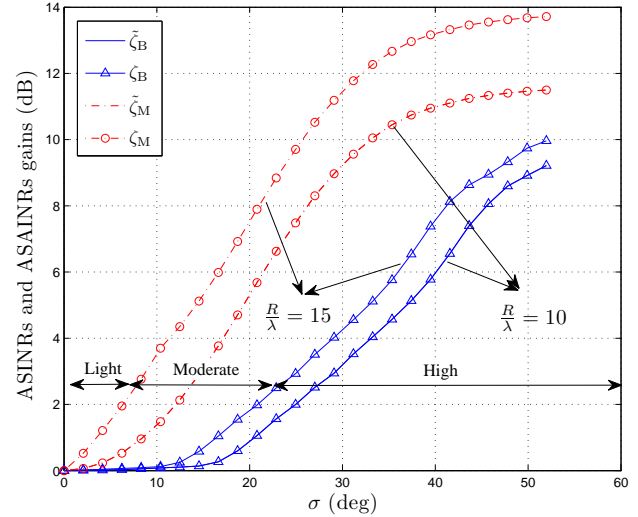


Fig. 5. ASINR and ASAINR gains of the proposed DZFB against its monochromatic and bichromatic benchmarks versus  $\sigma$  for  $K=20$  and different values of  $R/\lambda$ .

Qualitative Performance vs. Technique	Scattering Level in Interfered Environments		
	Light	Moderate	High
Monochromatic AFB	Low	Poor	Poor
Bichromatic AFB	Optimal	Optimal	Poor
Proposed DZFB	Optimal	Optimal	Optimal

Fig. 6. Qualitative performance of proposed DZFB and its distributed counterparts for different scattering levels in interfered environments.

terparts by dramatic ASINR gains of up to 14 and 10 dB, respectively, thereby confirming its net superiority.

Table 6 qualitatively summarizes the performance of each distributed AFB technique at light, moderate, and high scattering levels in interfered environments. It demonstrates that DZFB is filling a large gap in the literature by extending the applicability range of distributed AFB to highly-scattered environments where none of its distributed predecessors was able to achieve acceptable performance.

Fig. 7 illustrates the existing trade-off for WSN AFBs between the channel mismatch level they incur and the amount of overhead and power consumptions they require in highly-scattered and interfered environments. In highly-scattered and interfered environments, only the proposed DZFB is able to reach the target trade-off zone (i.e, low mismatch and overhead & power consumptions). However, as  $\sigma$  decreases, the bichromatic and monochromatic techniques move down towards the target zone. The bichromatic AFB would reach it first in moderately-scattered environments (i.e.,  $\sigma \leq 20$  deg) since the bichromatic channel approximation upon which it relies becomes then valid. In lightly-scattered environments

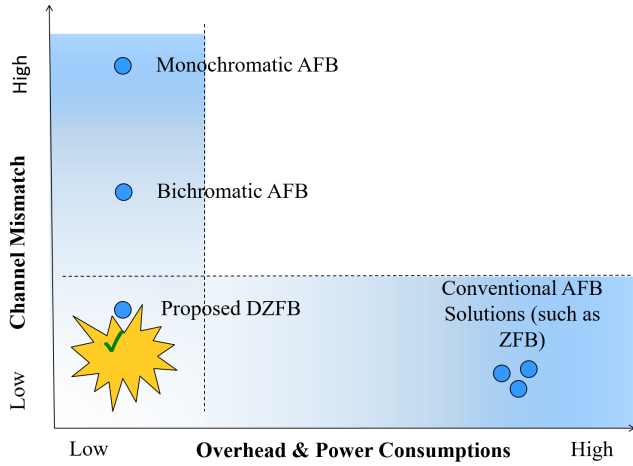


Fig. 7. Channel mismatch versus data exchange overhead and power consumption tradeoff in highly-scattered and interfered environments.

(i.e.,  $\sigma \leq 10$  deg), the monochromatic AFB joins the proposed and bichromatic techniques at the target zone. Furthermore, if  $K$  decreases the proposed DZFB experiences a minor performance loss of a dB fraction when  $K$  decreases as shown in Section VII. Consequently, it moves up in Fig. 7 while staying in the target zone. However, when  $K$  increases, the proposed DZFB performance reaches optimality whereas the conventional ZFB sees its overhead and power costs increase dramatically thereby moving even further to the right of Fig. 7.

### VIII. CONCLUSION

In this paper, OB was considered to establish a communication, through a WSN of  $K$  sensor nodes, from a source to a receiver in the presence of both scattering and interference. All sources send their data to the WSN during the first time slot while the nodes forward a properly weighted version of their received signals during the second slot. These ZFB weights are properly selected to maximize the desired power while completely canceling the interference signals. We showed that they depend on information locally unavailable at each node, making them unsuitable for WSNs from the prohibitive data exchange overhead and power depletion they would otherwise require. To address this issue, we exploit the asymptotic expression at large  $K$  of the ZFB weights that is locally computable at every node and, further, well-approximate their original counterparts. The performance of the resulting new DZFB version is analyzed and compared to ZFB and both monochromatic and bichromatic AFBs. We showed that DZFB is a best-of-two-words alternative for large  $\sigma$  that combines both advantages of its two counterparts (i.e., high performance and low overhead & power consumptions, respectively) while avoiding their weaknesses (i.e., low performance and high overhead & power consumptions, respectively).

### APPENDIX A

The power received at  $Rx$  from the  $m$ -th source located at  $\phi_m$  is defined as

$$\begin{aligned} \bar{P}_{w_P}(\phi_*) &= \mathbb{E} \left\{ |\mathbf{w}_P^H(\mathbf{f} \odot \mathbf{g}_*)|^2 \right\} \\ &= \frac{1}{K^2 (\beta_0 - \beta^H \mathbf{\Pi}^{-1} \beta)^2} \left( \mathbb{E} \{ \mathbf{h}_1^H \mathbf{h}_* \mathbf{h}_*^H \mathbf{h}_1 \} \right. \\ &\quad - \mathbb{E} \{ \mathbf{h}_1^H \mathbf{h}_* \mathbf{h}_*^H \mathbf{H}_1 \mathbf{\Pi}^{-1} \beta \} - \mathbb{E} \{ (\mathbf{h}_1^H \mathbf{h}_* \mathbf{h}_*^H \mathbf{H}_1 \mathbf{\Pi}^{-1} \beta)^* \} \\ &\quad \left. + \mathbb{E} \left\{ (\mathbf{H}_1 \mathbf{\Pi}^{-1} \beta)^H \mathbf{h}_* \mathbf{h}_*^H (\mathbf{H}_1 \mathbf{\Pi}^{-1} \beta) \right\} \right) \\ &= \frac{(\mathbb{E}(\Gamma_1) - \mathbb{E}(\Gamma_2) - \mathbb{E}(\Gamma_2^*) + \mathbb{E}(\Gamma_3))}{K^2 (\beta_0 - \beta^H \mathbf{\Pi}^{-1} \beta)^2}, \quad (37) \end{aligned}$$

where the expectation is taken over  $r_{k,s}$ ,  $\psi_{k,s}$ , and  $[\mathbf{f}]_{k,s}$  and  $\Gamma_1 = \mathbf{h}_1^H \mathbf{h}_* \mathbf{h}_*^H \mathbf{h}_1$ ,  $\Gamma_2 = \mathbf{h}_1^H \mathbf{h}_* \mathbf{h}_*^H \mathbf{H}_1 \mathbf{\Pi}^{-1} \beta$ , and  $\Gamma_3 = (\mathbf{H}_1 \mathbf{\Pi}^{-1} \beta)^H \mathbf{h}_* \mathbf{h}_*^H \mathbf{H}_1 \mathbf{\Pi}^{-1} \beta$ .

Let us first start by deriving the expression of  $\Gamma_1$  as (38) as shown in the top of the next page. On the other hand, we have (39) shown also in the top of the next page where  $x = \sin((\phi_* + \theta_{l,*} - \theta_{l',1})/2)$ ,  $x' = (\phi_* + \theta_{l,*} + \theta_{l',1})/2$ ,  $y = \sin((\theta_{l1,1} - \phi_* - \theta_{l2,*})/2)$ , and  $y' = (\theta_{l1,1} + \phi_* + \theta_{l2,*})/2$ . Exploiting the fact that  $r_p$ s and  $\psi_p$ s are mutually independent RV with pdfs

$$f_{r_p}(r) = \frac{2r}{R}, \quad 0 < r < R, \quad (40)$$

$$f_{\psi_p}(\psi) = \frac{1}{2\pi}, \quad -\pi \leq \psi < \pi, \quad (41)$$

respectively, we show that

$$\begin{aligned} \mathbb{E}_{\psi_p} \left( e^{-j \frac{4\pi}{\lambda} r_p (x \sin(x' - \psi_p) + y \sin(y' - \psi_p))} \right) &= \\ \frac{1}{2\pi} \int_{-\pi}^{\pi} e^{-j \frac{4\pi}{\lambda} r_p (x \sin(x' - \psi_p) + y \sin(y' - \psi_p))} d\psi_p &= \\ I_0 \left( -j \frac{4\pi}{\lambda} r_p \sqrt{x^2 + y^2 + 2xy \cos(x' - y')} \right) &= \\ J_0 \left( \frac{4\pi}{\lambda} r_p \sqrt{x^2 + y^2 + 2xy \cos(x' - y')} \right). \quad (42) \end{aligned}$$

By averaging this expression over  $r_p$ , we obtain

$$\begin{aligned} \mathbb{E}_{r_p, \psi_p} \left( e^{j \frac{4\pi}{\lambda} r_p (x \sin(x' - \psi_p) + y \sin(y' - \psi_p))} \right) &= \\ \mathbb{E}_{r_p} \left( J_0 \left( \frac{4\pi}{\lambda} r_p \sqrt{x^2 + y^2 + 2xy \cos(x' - y')} \right) \right) &= \\ \int_0^R \sum_{p=0}^{\infty} \frac{(-1)^p}{(p!)^2} \left( \frac{4\pi}{2\lambda} \right)^{2p} \sqrt{x^2 + y^2 + 2xy \cos(x' - y')}^{2p} &\times \\ \times (r_p)^{2p} \left( \frac{2r_p}{R} \right) dr_p &= \\ \sum_{p=0}^{\infty} \frac{(-1)^p}{p!(p+1)} \left( \frac{4\pi R \sqrt{x^2 + y^2 + 2xy \cos(x' - y')}}{2\lambda} \right)^{2p} &= \\ \frac{2\lambda J_1 \left( \frac{4\pi R}{\lambda} \sqrt{x^2 + y^2 + 2xy \cos(x' - y')} \right)}{4\pi R \sqrt{x^2 + y^2 + 2xy \cos(x' - y')}} &= \\ \Delta(\gamma_0(\phi_*)), \quad (43) \end{aligned}$$

$$\begin{aligned} \Gamma_1 &= \left( \sum_{p=1}^K \sum_{l,l'=1}^L \alpha_{l,\star} \alpha_{l',1}^* e^{-j \frac{2\pi}{\lambda} r_p [\cos(\phi_\star + \theta_{l,\star} - \psi_p) - \cos(\theta_{l',1} - \psi_p)]} \right) \left( \sum_{k=1}^K \sum_{l_1, l_2=1}^L \alpha_{l_1,1} \alpha_{l_2,\star}^* e^{-j \frac{2\pi}{\lambda} r_k [\cos(\theta_{l_1,1} - \psi_k) - \cos(\phi_\star + \theta_{l_2,\star} - \psi_k)]} \right) \\ &= \sum_{p=1}^K \sum_{l,l',l_1,l_2=1}^L \alpha_{l,\star} \alpha_{l',1}^* \alpha_{l_1,1} \alpha_{l_2,\star}^* e^{-j \frac{2\pi}{\lambda} r_p [\cos(\phi_\star + \theta_{l,\star} - \psi_p) - \cos(\theta_{l',1} - \psi_p) + \cos(\theta_{l_1,1} - \psi_p) - \cos(\phi_\star + \theta_{l_2,\star} - \psi_p)]} + \\ &\quad \sum_{p=1}^K \sum_{k=1, k \neq p}^K \sum_{l,l',l_1,l_2=1}^L \alpha_{l,\star} \alpha_{l',1}^* \alpha_{l_1,1} \alpha_{l_2,\star}^* e^{-j \frac{2\pi}{\lambda} r_p [\cos(\phi_\star + \theta_{l,\star} - \psi_p) - \cos(\theta_{l',1} - \psi_p)]} e^{-j \frac{2\pi}{\lambda} r_k [\cos(\theta_{l_1,1} - \psi_k) - \cos(\phi_\star + \theta_{l_2,\star} - \psi_k)]}. \end{aligned} \quad (38)$$

$$e^{-j \frac{4\pi}{\lambda} r_p (x \sin(x' - \psi_p) + y \sin(y' - \psi_p))} = e^{-j \frac{2\pi}{\lambda} r_p [\cos(\phi_\star + \theta_{l,\star} - \psi_p) - \cos(\theta_{l',1} - \psi_p)]} e^{-j \frac{2\pi}{\lambda} r_p [\cos(\theta_{l_1,1} - \psi_p) - \cos(\phi_\star + \theta_{l_2,\star} - \psi_p)]}, \quad (39)$$

where

$$\gamma_0(\phi_\star) = \arcsin \left( (x^2 + y^2 + 2xy \cos(x' - y'))^{1/2} \right). \quad (44)$$

Using (43) in (38) yields

$$E(\Gamma_1) = 2K \Sigma_0(\phi_\star) + 4K(K-1) \Sigma_1(\phi_\star) \Sigma_1^*(\phi_\star), \quad (45)$$

where

$$\Sigma_0(\phi_\star) = \sum_{l,l',l_1,l_2=1}^L \alpha_{l,\star} \alpha_{l',1}^* \alpha_{l_1,1} \alpha_{l_2,\star}^* \Delta(2\gamma_0(\phi_\star)), \quad (46)$$

and

$$\Sigma_1(\phi_\star) = \sum_{l,l'=1}^L \alpha_{l,\star} \alpha_{l',1}^* \Delta(\theta_{l,\star} - \theta_{l',1} + \phi_\star). \quad (47)$$

Following the above approach, we can also obtain

$$\begin{aligned} E(\Gamma_2) &= 2K \Sigma_2^H(\phi_\star) \mathbf{\Pi}^{-1} \boldsymbol{\beta} + 4K(K-1) \Sigma_1(\phi_\star) \\ &\quad \times \Sigma_4^H(\phi_\star) \mathbf{\Pi}^{-1} \boldsymbol{\beta}, \end{aligned} \quad (48)$$

where

$$[\Sigma_2(\phi_\star)]_p = \sum_{l,l',l_1,l_2=1}^L \alpha_{l,\star} \alpha_{l',p+1}^* \alpha_{l_1,\star} \alpha_{l_2,p+1}^* \Delta(2\gamma_1(\theta, \phi_{p+1}, \phi_\star)), \quad (49)$$

$$\begin{aligned} \gamma_1(\phi_p, \phi_\star) &= \arcsin \left( (x^2 + y_1^2 + 2xy_1 \cos(x' - y_1'))^{1/2} \right), \\ y_1 &= \sin(\phi_p + \theta_{l_1,p} - \phi_\star - \theta_{l_2,\star})/2, \quad y_1' = \\ &= (\phi_p + \theta_{l_1,p} + \phi_\star + \theta_{l_2,\star})/2, \quad \text{and } [\Sigma_4(\phi_\star)]_p = \\ &= \sum_{l,l'=1}^L \alpha_{l,\star} \alpha_{l',p+1}^* \Delta(\theta_{l,\star} - \theta_{l',p+1} + \phi_\star - \phi_{p+1}). \end{aligned}$$

As far as  $E(\Gamma_3)$  is concerned, it can be expressed as

$$\begin{aligned} E(\Gamma_3) &= 2K \boldsymbol{\beta}^H \mathbf{\Pi}^{-1} \Sigma_3(\phi_\star) \mathbf{\Pi}^{-1} \boldsymbol{\beta} + 4K(K-1) \boldsymbol{\beta}^H \mathbf{\Pi}^{-1} \\ &\quad \times \Sigma_4(\phi_\star) \Sigma_4^H(\phi_\star) \mathbf{\Pi}^{-1} \boldsymbol{\beta}, \end{aligned} \quad (50)$$

where

$$\begin{aligned} [\Sigma_3(\phi_\star)]_{pq} &= \sum_{l,l',l_1,l_2=1}^L \alpha_{l,p+1} \alpha_{l',q+1}^* \alpha_{l_1,q+1} \alpha_{l_2,p+1}^* \\ &\quad \times \Delta(2\gamma_2(\theta, \phi_{p+1}, \phi_{q+1}, \phi_\star)), \end{aligned} \quad (51)$$

$$\begin{aligned} \gamma_2(\phi_p, \phi_q, \phi_\star) &= \arcsin \left( (x_1^2 + y_1^2 + 2x_1y_1 \cos(x_1' - y_1'))^{1/2} \right) \\ , \quad x_1 &= \sin(\phi_\star + \theta_{l,p} - \phi_q - \theta_{l',q})/2, \quad x_1' = (\phi_\star + \theta_{l,p} + \phi_q + \\ &+ \theta_{l',q})/2, \quad y_1 = \sin(\phi_p + \theta_{l_1,q} - \phi_\star - \theta_{l_2,p})/2, \quad \text{and } y_1' = \\ &= (\phi_p + \theta_{l_1,q} + \phi_\star + \theta_{l_2,p})/2. \quad \text{Substituting (45), (48), and (50)} \\ &\text{in (37) yields to (21).} \end{aligned}$$

## APPENDIX B

From (27), we have

$$\bar{P}_{\mathbf{w}_B}(\phi_\star) = \frac{E\{\eta_1\} - E\{\eta_2\} - E\{\eta_2^*\} + E\{\eta_3\}}{K^2(1 + \Delta(2\sigma_1) - \boldsymbol{\beta}_B^T \mathbf{\Pi}^{-1} \boldsymbol{\beta}_B)}, \quad (52)$$

where  $\eta_1 = \boldsymbol{\beta}_B^T \mathbf{\Pi}_B^{-1} \mathbf{H}_{B,I}^H \mathbf{h}_{B,m} \mathbf{h}_m^H \mathbf{H}_{B,I} \mathbf{\Pi}_B^{-1} \boldsymbol{\beta}_B$ ,  $\eta_2 = \mathbf{h}_{B,1}^H \mathbf{h}_{B,m} \mathbf{h}_m^H \mathbf{H}_{B,I} \mathbf{\Pi}_B^{-1} \boldsymbol{\beta}_B$ , and  $\eta_3 = \mathbf{h}_{B,1}^H \mathbf{h}_{B,m} \mathbf{h}_m^H \mathbf{h}_{B,1}$ .

Let us first focus on  $E\{\eta_3\}$ . According to (i), we have

$$\begin{aligned} E_{\alpha_{l,m}}\{\eta_1\} &= \sum_{l=1}^L \frac{1}{L} \left( \boldsymbol{\beta}_B^T \mathbf{\Pi}_B^{-1} \mathbf{H}_{B,I}^H \mathbf{g}_m^{(1)}(\phi_m + \theta_{l,m}) \right) \\ &\quad \times \left( \mathbf{g}_m^{(1)}(\phi_m + \theta_{l,m})^H \mathbf{H}_{B,I} \mathbf{\Pi}_B^{-1} \boldsymbol{\beta}_B \right) \\ &= \sum_{l=1}^L \frac{1}{L} \left( \sum_{p=1}^{2M-2} [\boldsymbol{\beta}_B^T \mathbf{\Pi}_B^{-1}]_p [\mathbf{\Pi}_B^{-1} \boldsymbol{\beta}_B]_p \varepsilon_p \right. \\ &\quad \left. + \sum_{p=1}^{2M-2} \sum_{n=1, n \neq p}^{2M-2} [\boldsymbol{\beta}_B^T \mathbf{\Pi}_B^{-1}]_p [\mathbf{\Pi}_B^{-1} \boldsymbol{\beta}_B]_n \delta_{p,n} \right), \end{aligned} \quad (53)$$

where  $\varepsilon_p = [\mathbf{H}_{B,I}^H \mathbf{g}_m^{(1)}(\phi_m + \theta_{l,m})]_p [\mathbf{g}_m^{(1)}(\phi_m + \theta_{l,m})^H \mathbf{H}_{B,I}]_p$

and  $\delta_{p,n} = [\mathbf{H}_{B,I}^H \mathbf{g}_m^{(1)}(\phi_m + \theta_{l,m})]_p [\mathbf{g}_m^{(1)}(\phi_m + \theta_{l,m})^H \mathbf{H}_{B,I}]_n$ .  $\varepsilon_p$  could be equivalently rewritten as

$$\begin{aligned} \varepsilon_p &= \left( \sum_{k=1}^K [\mathbf{H}_{B,I}^H]_{pk} [\mathbf{g}_m^{(1)}(\phi_m + \theta_{l,m})]_k \right) \\ &\quad \left( \sum_{s=1}^K [\mathbf{g}_m^{(1)}(\phi_m + \theta_{l,m})^H]_s [\mathbf{H}_{B,I}]_{sp} \right) \\ &= K + \sum_{k=1}^K e^{-j4\pi \frac{R}{\lambda} \sin\left(\frac{\phi_m + \theta_{l,m} - \bar{\phi}_p}{2}\right)} \sin\left(\psi_k - \frac{\phi_m + \theta_{l,m} + \bar{\phi}_p}{2}\right) \\ &\quad \times \sum_{s=1, s \neq k}^K e^{j4\pi \frac{R}{\lambda} \sin\left(\frac{\phi_m + \theta_{l,m} - \bar{\phi}_p}{2}\right)} \sin\left(\psi_k - \frac{\phi_m + \theta_{l,m} + \bar{\phi}_p}{2}\right). \end{aligned} \quad (54)$$

Exploiting the fact that  $r_k$ s and  $\psi_k$ s are i.i.d random variables and  $(2/\pi) \int_{-1}^1 e^{j4\pi \frac{R}{\lambda} \sin(\frac{\phi}{2})z} \sqrt{1-z^2} dz = \Delta(\phi)$ , we show

$$\mathbb{E}_{\alpha_{l,m}, r_k, \psi_k} \{\eta_3\} = \sum_{l=1}^L \frac{2K\beta_B^T \mathbf{\Pi}_B^{-1} \beta_B + 4K(K-1) \left( \frac{J_1(\gamma(\phi_m + \theta_{l,m} + \sigma_1))}{\gamma(\phi_m + \theta_{l,m} + \sigma_1)} + \frac{J_1(\gamma(\phi_m + \theta_{l,m} - \sigma_1))}{\gamma(\phi_m + \theta_{l,m} - \sigma_1)} \right)^2}{L}. \quad (59)$$

that

$$\begin{aligned} \mathbb{E}_{r_k, \psi_k} \{\varepsilon_p\} &= K + 2K(K-1) [\boldsymbol{\tau}_B(\phi_m + \theta_{l,m})]_p \\ &\times [\boldsymbol{\tau}_B^T(\phi_m + \theta_{l,m})]_p. \end{aligned} \quad (55)$$

We also show that

$$\begin{aligned} \mathbb{E}_{\alpha_{l,m}, r_k, \psi_k} \{\delta_{p,n}\} &= 2K(K-1) [\boldsymbol{\tau}_B(\phi_m + \theta_{l,m})]_p \\ &\times [\boldsymbol{\tau}_B^T(\phi_m + \theta_{l,m})]_n + 2K [\mathbf{\Pi}_B]_{pq}. \end{aligned} \quad (56)$$

It follows then from (55) and (56) that

$$\begin{aligned} \mathbb{E}_{\alpha_{l,m}, r_k, \psi_k} \{\eta_1\} &= \sum_{l=1}^L \frac{1}{L} \left( 2K\beta_B^T \mathbf{\Pi}_B^{-1} \beta_B + 4K(K-1) \right. \\ &\times \left. \left( \boldsymbol{\tau}_B^T(\phi_m + \theta_{l,m}) \mathbf{\Pi}_B^{-1} \beta_B \right)^2 \right), \end{aligned} \quad (57)$$

since  $[\mathbf{\Pi}_B]_{pp} = 1/2$ . Furthermore, following the same approach above, we prove that

$$\begin{aligned} \mathbb{E}_{\alpha_{l,m}, r_k, \psi_k} \{\eta_2\} &= \sum_{l=1}^L \frac{1}{L} \left( 2K\beta_B^T \mathbf{\Pi}_B^{-1} \beta_B + 4K(K-1) \right. \\ &\times \left. \left( \frac{J_1(\gamma(\phi_m + \theta_{l,m} + \sigma_1))}{\gamma(\phi_m + \theta_{l,m} + \sigma_1)} + \frac{J_1(\gamma(\phi_m + \theta_{l,m} - \sigma_1))}{\gamma(\phi_m + \theta_{l,m} - \sigma_1)} \right) \right. \\ &\times \left. \boldsymbol{\tau}_B^T(\phi_m + \theta_{l,m}) \mathbf{\Pi}_B^{-1} \right), \end{aligned} \quad (58)$$

and (59) as shown on the top of the next page. Note that  $\mathbb{E}_{\alpha_{l,m}, r_k, \psi_k} \{\eta_2\} = \mathbb{E}_{\alpha_{l,m}, r_k, \psi_k} \{\eta_2^*\}$  since  $\mathbb{E}_{r_k, \psi_k} \{\eta_2\}$  is real. Finally, applying the expectation with respect to  $\theta_{l,m}$ s over both sides of (57)-(59) and substituting the resulting equations in (52),  $\bar{P}_{\mathbf{w}_B}(\phi_*)$  is obtained.

Now let us focus on  $\bar{P}_{\mathbf{w}_M}(\phi_*)$ . It can be observed from (26) and (27) that  $\mathbf{w}_B$  boils down, as expected, to  $\mathbf{w}_M$  when  $\sigma_m = 0$ ,  $m = 1, \dots, M$  (i.e., there is no scattering). Therefore, by substituting  $\sigma_m$ s with 0 in (28),  $\bar{P}_{\mathbf{w}_M}(\phi_*)$  is obtained as in (30).

## APPENDIX C

In order to verify (36), one should derive  $\mathbb{E}\{\lim_{K \rightarrow \infty} P_{\mathbf{w}_P}\}$  and  $\mathbb{E}\{\lim_{K \rightarrow \infty} N_{\mathbf{w}}\}$ . Let us first focus on  $\mathbf{w} = \mathbf{w}_P$ . From (37), we have

$$\begin{aligned} \mathbb{E}\left\{\lim_{K \rightarrow \infty} P_{\mathbf{w}_P}(\phi_*)\right\} &= \frac{\mathbb{E}(\lim_{K \rightarrow \infty} \Gamma_1) - \mathbb{E}(\lim_{K \rightarrow \infty} \Gamma_2)}{K^2 \left( \beta_0 - \beta^H \mathbf{\Pi}^{-1} \beta \right)^2} \\ &\quad - \frac{\mathbb{E}(\lim_{K \rightarrow \infty} \Gamma_2^*) - \mathbb{E}(\lim_{K \rightarrow \infty} \Gamma_3)}{K^2 \left( \beta_0 - \beta^H \mathbf{\Pi}^{-1} \beta \right)^2}. \end{aligned} \quad (60)$$

It follows from (38) that we have (61) as shown on the top of the page. Using the strong (39) along with LLN on the RHS

of (61) yields

$$\begin{aligned} \lim_{K \rightarrow \infty} \Gamma_1 &= \sum_{l, l', l_1, l_2=1}^L \alpha_{l,*} \alpha_{l',1}^* \alpha_{l_1,1} \alpha_{l_2,*}^* \\ &\left( \mathbb{E}\left\{ e^{-j \frac{2\pi}{\lambda} r_p} [\cos(\phi_* + \theta_{l,*} - \psi_p) - \cos(\theta_{l',1} - \psi_p)] \right\} \right. \\ &\times \left. \mathbb{E}\left\{ e^{-j \frac{2\pi}{\lambda} r_k} [\cos(\theta_{l_1,1} - \psi_k) - \cos(\phi_* + \theta_{l_2,*} - \psi_k)] \right\} \right) \\ &= 4\Sigma_1(\phi_*) \Sigma_1^*(\phi_*). \end{aligned} \quad (62)$$

Following similar steps, we show

$$\lim_{K \rightarrow \infty} \Gamma_2 = 4\Sigma_1(\phi_*) \Sigma_4^H(\phi_*) \mathbf{\Pi}^{-1} \beta, \quad (63)$$

and

$$\lim_{K \rightarrow \infty} \Gamma_3 = 4\Sigma_1(\phi_*) \Sigma_4^H(\phi_*) \mathbf{\Pi}^{-1} \beta. \quad (64)$$

Furthermore, we have

$$N_{\mathbf{w}_P} = \sigma_v^2 \mathbf{w}_P^H \mathbf{\Lambda} \mathbf{w}_P + \sigma_n^2. \quad (65)$$

where  $\mathbf{\Lambda} \triangleq \text{diag}\{|\mathbf{f}|_1|^2 \dots |\mathbf{f}|_K|^2\}$ . Exploiting (14), (16), and (17), we can easily show that

$$\begin{aligned} \lim_{K \rightarrow \infty} N_{\mathbf{w}_P} &= \lim_{K \rightarrow \infty} \frac{\sigma_v^2}{K^2 \left( \beta_0 - \beta^H \mathbf{\Pi}^{-1} \beta \right)} + \sigma_n^2 \\ &= \sigma_n^2. \end{aligned} \quad (66)$$

From (62)-(66), the asymptotic  $\tilde{\gamma}_{\mathbf{w}_P}$  can be expressed as

$$\begin{aligned} \lim_{K \rightarrow \infty} \tilde{\gamma}_{\mathbf{w}_P} &= \frac{1}{\sigma_n^2} \\ &= \lim_{K \rightarrow \infty} \tilde{\gamma}_{\mathbf{w}_P}. \end{aligned} \quad (67)$$

Let us now focus on  $\mathbf{w} = \mathbf{w}_B$ . It is direct to show from (52) that

$$\begin{aligned} \mathbb{E}\left\{\lim_{K \rightarrow \infty} P_{\mathbf{w}_B}(\phi_*)\right\} &= \frac{\mathbb{E}(\lim_{K \rightarrow \infty} \eta_1) - \mathbb{E}(\lim_{K \rightarrow \infty} \eta_2)}{K^2 \left( 1 + \Delta(2\sigma_1) - \beta_B^T \mathbf{\Pi}^{-1} \beta_B \right)^2} \\ &\quad - \frac{\mathbb{E}(\lim_{K \rightarrow \infty} \eta_2^*) - \mathbb{E}(\lim_{K \rightarrow \infty} \eta_3)}{K^2 \left( 1 + \Delta(2\sigma_1) - \beta_B^T \mathbf{\Pi}^{-1} \beta_B \right)^2}. \end{aligned} \quad (68)$$

It follows from the definition of  $\eta_1$  that  $\lim_{K \rightarrow \infty} \eta_1$  can be expressed as (69) as shown on the top of the page. Exploiting the strong LLN, one can prove that

$$\lim_{K \rightarrow \infty} \frac{1}{K} \mathbf{H}_{B, \mathbf{I}}^H \mathbf{g}_m^{(1)}(\phi) = 2\boldsymbol{\tau}_B(\phi). \quad (70)$$

Substituting (70) in (69) and applying the expectation with respect to  $\alpha_{l,m}$  over the resulting equation yields

$$\begin{aligned} \mathbb{E}_{\alpha_l} \left\{ \lim_{K \rightarrow \infty} \eta_1 \right\} &= \frac{\sum_{l=1}^L \frac{4}{L} \left( \boldsymbol{\tau}_B^T(\phi_m + \theta_{l,m}) \mathbf{\Pi}_B^{-1} \beta_B \right)^2}{\left( 1 + \Delta(2\sigma_1) - \beta_B^T \mathbf{\Pi}^{-1} \beta_B \right)^2}. \end{aligned} \quad (71)$$

$$\begin{aligned}
 \lim_{K \rightarrow \infty} \Gamma_1 &= \frac{1}{\left(\beta_0 - \beta^H \mathbf{\Pi}^{-1} \beta\right)} \left( \left( \lim_{K \rightarrow \infty} \frac{1}{K} \right) \sum_{l, l', l_1, l_2=1}^L \alpha_{l, \star} \alpha_{l', 1}^* \alpha_{l_1, 1} \alpha_{l_2, \star}^* \times \right. \\
 &\lim_{K \rightarrow \infty} \sum_{p=1}^K \frac{1}{K} \times e^{-j \frac{2\pi}{\lambda} r_p [\cos(\phi_{\star} + \theta_{l, \star} - \psi_p) - \cos(\theta_{l', 1} - \psi_p) + \cos(\theta_{l_1, 1} - \psi_p) - \cos(\phi_{\star} + \theta_{l_2, \star} - \psi_p)]} \left. + \right. \\
 &\left( \lim_{K \rightarrow \infty} \frac{K(K-1)}{K^2} \right) \sum_{l, l', l_1, l_2=1}^L \alpha_{l, \star} \alpha_{l', 1}^* \alpha_{l_1, 1} \alpha_{l_2, \star}^* \lim_{K \rightarrow \infty} \frac{1}{K} \sum_{p=1}^K e^{-j \frac{2\pi}{\lambda} r_p [\cos(\phi_{\star} + \theta_{l, \star} - \psi_p) - \cos(\theta_{l', 1} - \psi_p)]} \times \\
 &\left. \lim_{K \rightarrow \infty} \sum_{k=1, k \neq p}^K \frac{1}{(K-1)} e^{-j \frac{2\pi}{\lambda} r_k [\cos(\theta_{l_1, 1} - \psi_k) - \cos(\phi_{\star} + \theta_{l_2, \star} - \psi_k)]} \right). \quad (61)
 \end{aligned}$$

$$\lim_{K \rightarrow \infty} \eta_1 = \frac{\sum_{l, l'=1}^L \alpha_{l, \star} \alpha_{l', 1} \left( \beta_B^T \mathbf{\Pi}_B^{-1} \lim_{K \rightarrow \infty} \left( \frac{\mathbf{H}_{B,1}^H \mathbf{g}_m^{(1)}(\phi_m + \theta_{l, m})}{K} \right) \right) \left( \lim_{K \rightarrow \infty} \frac{\left( \mathbf{g}_m^{(1)}(\phi_m + \theta_{l', 1})^H \mathbf{H}_{B,1} \right)}{K} \mathbf{\Pi}_B^{-1} \beta_B \right)}{\left( 1 + \Delta(2\sigma_1) - \beta_B^T \mathbf{\Pi}_B^{-1} \beta_B \right)^2}. \quad (69)$$

Please note that we exploit in (71) the fact that  $E\{\alpha_l \alpha_{l'}^*\} = 1$  if  $l = l'$  and 0 otherwise, as stated in assumption (i). Following the same derivation steps above, it can be shown that

$$\begin{aligned}
 E_{\alpha_l} \left\{ \lim_{K \rightarrow \infty} \eta_2 \right\} &= \frac{1}{\left( 1 + \Delta(2\sigma_1) - \beta_B^T \mathbf{\Pi}_B^{-1} \beta_B \right)^2} \\
 &\sum_{l=1}^L \frac{8}{L} \left( \Delta(\phi_m + \theta_{l, m} + \sigma_1) + \Delta(\phi_m + \theta_{l, m} - \sigma_1) \right) \\
 &\times \tau_B^T(\phi_m + \theta_{l, m}) \mathbf{\Pi}_B^{-1}, \quad (72)
 \end{aligned}$$

$$\begin{aligned}
 E_{\alpha_l} \left\{ \lim_{K \rightarrow \infty} \eta_3 \right\} &= \frac{1}{\left( 1 + \Delta(2\sigma_1) - \beta_B^T \mathbf{\Pi}_B^{-1} \beta_B \right)^2} \\
 &\sum_{l=1}^L \frac{4}{L} \left( \Delta(\phi_m + \theta_{l, m} + \sigma_1) + \Delta(\phi_m + \theta_{l, m} - \sigma_1) \right)^2, \quad (73)
 \end{aligned}$$

and

$$E_{\alpha_l} \left\{ \lim_{K \rightarrow \infty} N_{\mathbf{w}_B} \right\} = \sigma_n^2. \quad (74)$$

Applying the expectation with respect to  $\theta_{l, m}$  over (71)-(74) and using the resulting equations yields

$$\begin{aligned}
 \lim_{K \rightarrow \infty} \tilde{\gamma}_{\mathbf{w}_B} &= \frac{\Psi_B(0)}{4 \left( 1 + \Delta(2\sigma_1) - \beta_B^T \mathbf{\Pi}_B^{-1} \beta_B \right)^2} \\
 &= \lim_{K \rightarrow \infty} \gamma_{\mathbf{w}_B}. \quad (75)
 \end{aligned}$$

The same approach can be applied to show that

$$\begin{aligned}
 \lim_{K \rightarrow \infty} \tilde{\gamma}_{\mathbf{w}_M} &= \frac{\Psi_M(0)}{4 \left( 1 - \beta_M^T \mathbf{\Pi}_M^{-1} \beta_M \right)^2} \\
 &= \lim_{K \rightarrow \infty} \gamma_{\mathbf{w}_M}. \quad (76)
 \end{aligned}$$

## REFERENCES

- [1] S. Jayaprakasam, S. K. A. Rahim, and C. Y. Leow, "Distributed and collaborative beamforming in wireless sensor networks: classifications, trends, and research directions," *IEEE Commun. Surveys & Tutorials*, vol. 19, pp. 2092-2116, June 2017.
- [2] H. Ochiai, P. Mitran, H. Poor, and V. Tarokh, "Collaborative beamforming for distributed wireless ad hoc sensor networks," *IEEE Trans. Sig. Process.*, vol. 53, pp. 4110-4124, November 2005.
- [3] X. Shen, J. Huang, P. Liu, Y. Pan, B. Xu, and Z. Rao, "Analysis of collaborative beamforming for wireless sensor networks with phase offset," *Radioengineering*, vol. 23, pp. 421-429, April 2014.
- [4] M. F. A. Ahmed, and S. A. Vorobyov, "Collaborative beamforming for wireless sensor networks with Gaussian distributed sensor nodes," *IEEE Trans. Wireless Commun.*, vol. 8, pp. 638-643, February 2009.
- [5] J. Huang, P. Wang, and Q. Wan, "Collaborative beamforming for wireless sensor networks with arbitrary distributed sensors," *IEEE Commun. Lett.*, vol. 16, pp. 1118-1120, July 2012.
- [6] K. Zarifi, A. Ghayeb, and S. Affes, "Distributed beamforming for wireless sensor networks with improved graph connectivity and energy efficiency," *IEEE Trans. Sig. Process.*, vol. 58, pp. 1904-1921, March 2010.
- [7] C. H. Wong, Z. W. Siew, M. K. Tan, R. K. Y. Chin, and K. T. K. Teo, "Optimization of distributed and collaborative beamforming in wireless sensor networks," *IEEE CICSyN'2012*, Phuket, Thailand, July 24-26 2012.
- [8] M. Ahmed and S. Vorobyov, "Sidelobe control in collaborative beamforming via node selection," *IEEE Trans. Sig. Process.*, vol. 58, pp. 6168-6180, December 2010.
- [9] R. Mudumbai, G. Barriac, and U. Madhow, "On the feasibility of distributed beamforming in wireless networks," *IEEE Trans. Wireless Comm.*, vol. 6, pp. 1754-1763, May 2007.
- [10] D. R. Brown and H. Poor, "Time-slotted round trip carrier synchronization for distributed beamforming," *IEEE Trans. on Sig. Process.*, vol. 56, pp. 5630-5643, November 2008.
- [11] H. Ochiai, P. Mitran, H. V. Poor, and V. Tarokh, "Collaborative beamforming in ad hoc networks," *IEEE ITW 2004*, San Antonio, TX, USA, October 24-29 2004.
- [12] L. C. Godara, "Application of antenna arrays to mobile communications, part II: beam-forming and direction-of-arrival considerations," *Proc. on the IEEE*, vol. 85, pp. 1195-1245, August 1997.
- [13] R. Mudumbai, D. R. Brown, U. Madhow, and H. Poor, "Distributed transmit beamforming: challenges and recent progress," *IEEE Commun. Mag.*, vol. 47, pp. 102-110, February 2009.
- [14] NNN. A. Malik, M. Esa, SK. Yusof, and NM. A. Latiff, "Collaborative beamforming null-steering array for wireless sensor networks," *Proc. IEEE ISTT'2014*, Langkawi, Malaysia, November 24-26 2014.

- [15] L. Dong, A. P. Petropulu, and H. V. Poor, "A cross-layer approach to collaborative beamforming for wireless ad hoc networks," *IEEE Trans. Sig. Process.*, vol. 56, pp. 2981-2993, July 2008.
- [16] D. Astly and B. Ottersten, "The effects of local scattering on direction of arrival estimation with MUSIC," *IEEE Trans. Sig. Process.*, vol. 47, pp. 3220-3234, December 1999.
- [17] O. Besson, P. Stoica, and A. Gershman, "Simple and accurate direction of arrival estimator in the case of imperfect spatial coherence," *IEEE Trans. Sig. Process.*, vol. 49, pp. 730-737, April 2001.
- [18] S. Shahbazpanahi, S. Valaee, and A. Gershman, "A covariance fitting approach to parametric localization of multiple incoherently distributed sources," *IEEE Trans. Sig. Process.*, vol. 52, pp. 592-600, March 2004.
- [19] M. Souden, S. Affes, and J. Benesty, "A two-stage approach to estimate the angles of arrival and the angular spreads of locally scattered sources," *IEEE Trans. Sig. Process.*, vol. 56, pp. 1968-1983, May 2008.
- [20] M. Bengtsson and B. Ottersten, "Low-complexity estimators for distributed sources," *IEEE Trans. Sig. Process.*, vol. 48, pp. 2185-2194, August 2000.
- [21] A. Amar, "The effect of local scattering on the gain and beamwidth of a collaborative beampattern for wireless sensor networks," *IEEE Trans. Wireless Commun.*, vol. 9, pp. 2730-2736, September 2010.
- [22] S. Zaidi and S. Affes, "Distributed collaborative beamforming in the presence of angular scattering," *IEEE Trans. Commun.*, vol. 62, pp. 1668-1680, May 2014.
- [23] S. Zaidi and S. Affes, "Distributed collaborative beamforming design for maximized throughput in interfered and scattered environments," *IEEE Trans. Commun.*, vol. 63, pp. 4905-4919, December 2015.
- [24] S. Zaidi, O. B. Smida, S. Affes, and S. Valaee, "Energy-Efficient distributed amplify-and-forward beamforming for wireless sensor networks," *Proc. IEEE CAMSAP'2017*, Curacao, Netherlands Antilles, December 10-13 2017.
- [25] H. Shen, W. Xu, S. Jin, and C. Zhao, "Joint transmit and receive beamforming for MIMO downlinks with channel uncertainty," *IEEE Trans. Veh. Tech.*, vol. 63, pp. 2319-2335, June 2014.
- [26] Z. Yi and I. Kim, "Joint optimization of relay-precoders and decoders with partial channel side information in cooperative networks," *IEEE Journal on Selected Areas in Commun.*, vol. 25, pp. 447-458, February 2007.
- [27] Y. Jing and H. Jafarkhani, "Network beamforming using relays with perfect channel information," *IEEE Trans. on Information Theory*, vol. 55, pp. 2499-2517, June 2009.
- [28] H.-B. Kong, C. Song, H. Park, and I. Lee, "A new beamforming design for MIMO AF relaying systems with direct link," *IEEE Trans. Commun.*, vol. 62, pp. 2286-2295, July 2014.
- [29] S. Zaidi and S. Affes, "SNR and throughput analysis of distributed collaborative beamforming in locally-scattered environments," *Wiley J. Wireless Commun. and Mobile Comput.*, vol. 12, pp. 1620-1633, December 2012.
- [30] M. Zeng, R. Zhang, and S. Cui, "On design of collaborative beamforming for two-way relay networks," *IEEE Trans. Sig. Process.*, vol. 59, pp. 2284-2295, May 2011.
- [31] K. Zarifi, S. Zaidi, S. Affes, and A. Ghayeb, "A distributed amplify-and-forward beamforming technique in wireless sensor networks," *IEEE Trans. Signal Process.*, vol. 59, pp. 3657-3674, August 2011.
- [32] L. Dong, A. P. Petropulu, and H. V. Poor, "Weighted cross-layer cooperative beamforming for wireless networks," *IEEE Trans. on Sig. Proc.*, vol. 57, pp. 3240-3252, August 2009.?